

# Experiments and Modeling of the Autoignition of Methyl Valerate at Low to Intermediate Temperatures and Elevated Pressures in a Rapid Compression Machine

Bryan W. Weber<sup>a,\*</sup>, Justin A. Bunnell<sup>a</sup>, Kamal Kumar<sup>b</sup>, Chih-Jen Sung<sup>a</sup>

<sup>a</sup>*Department of Mechanical Engineering, University of Connecticut, Storrs, CT, USA*

<sup>b</sup>*Department of Mechanical Engineering, University of Idaho, Moscow, ID, USA*

---

## Abstract

Methyl valerate ( $\text{C}_6\text{H}_{12}\text{O}_2$ , methyl pentanoate) is a methyl ester and a relevant surrogate component for biodiesel. In this work, we present ignition delays of methyl valerate measured using a rapid compression machine at a range of engine-relevant temperature, pressure, and equivalence ratio conditions. The conditions we have studied include equivalence ratios ( $\phi$ ) from 0.25 to 2.0, temperatures between 680 K and 1050 K, and pressures of 15 bar and 30 bar. The ignition delay data demonstrate a negative temperature coefficient region in the temperature range of 720 K–800 K for both  $\phi = 2.0$ , 15 bar and  $\phi = 1.0$ , 30 bar, with two-stage ignition apparent over the narrower temperature ranges of 720 K–760 K for 15 bar and 740 K–760 K at 30 bar. In addition, the experimental ignition delay data are compared with simulations using an existing chemical kinetic model from the literature. The simulations with the literature model under-predict the data by factors between 2 and 10 over the entire range of the experimental data. In addition, a new chemical kinetic model is developed using the Reaction Mechanism Generator (RMG) software. The agreement between the experimental data and the RMG model is also not satisfactory. To help determine the possible reasons for the disagreement, a path analysis of both models is completed. It is found that improvements to both the reaction

---

\*Corresponding Author: bryan.weber@uconn.edu

pathways and thermodynamic properties are required. Further directions for future improvement of the methyl valerate model are discussed.

*Keywords:* chemical kinetics, rapid compression machine, autoignition, methyl ester, methyl valerate, methyl pentanoate

---

## 1. Introduction

For transportation applications, biodiesel is an important constituent in improving environmental friendliness of fuels. This is due to its renewability when produced from sustainable agricultural crops and its ability to reduce emissions relative to petroleum-derived fuels [1]. Biodiesel typically consists of long-chain methyl ester molecules, with typical compositions of  $C_{14}$  to  $C_{20}$  [1]. Recognizing that the large molecular size of the methyl esters within biodiesel fuel makes creating and using detailed chemical kinetic models challenging [2], it is desired to study their combustion chemistry by studying simpler methyl ester molecules.

A recent review paper summarizes the work on methyl esters relevant to biodiesel combustion [3]; the following summary focuses on ignition delay measurements, since these are the focus of this paper. Autoignition of methyl butanoate (MB,  $C_5H_{10}O_2$ ) has been well-studied in both shock tube and rapid compression machine experiments [4–10]. The prevalence of MB data in the literature is largely due to the early identification of MB as a potential surrogate fuel for biodiesel [11]. However, the experiments have shown that MB may not be an appropriate surrogate for biodiesel, due to its lack of negative temperature coefficient (NTC) behavior, a requirement for a suitable biodiesel surrogate [3].

Methyl esters larger than MB, such as methyl valerate (MV,  $C_6H_{12}O_2$ , methyl pentanoate), have also been studied as possible biodiesel surrogates. Hadj-Ali et al. [9] used a rapid compression machine (RCM) to study the autoignition of several methyl esters including MV. Although MV exhibited two-stage ignition in this study, little additional research has been done on its low-temperature chemistry. Korobeinichev et al. [12] studied MV in premixed lam-

26 inar flames and extended a detailed high temperature chemical kinetic model  
 27 to include MV and methyl hexanoate. Dmitriev et al. [13] added MV to n-  
 28 heptane/toluene fuel blends to determine the resulting intermediate species in  
 29 premixed flames using a flat burner at 1 atm and an equivalence ratio of 1.75.  
 30 The addition of MV helped reduce soot forming intermediates including ben-  
 31 zene, cyclopentadienyl, acetylene, propargyl, and vinylacetylene [13]. Hayes  
 32 and Burgess [14] computationally examined the peroxy radical isomerization  
 33 reactions for MV to better understand the low temperature reaction pathways.  
 34 Finally, Diévert et al. [15] used diffusion flames in the counterflow configuration  
 35 to determine extinction limits for a number of methyl esters, including MV, and  
 36 validated a detailed kinetic model with the experimental data.

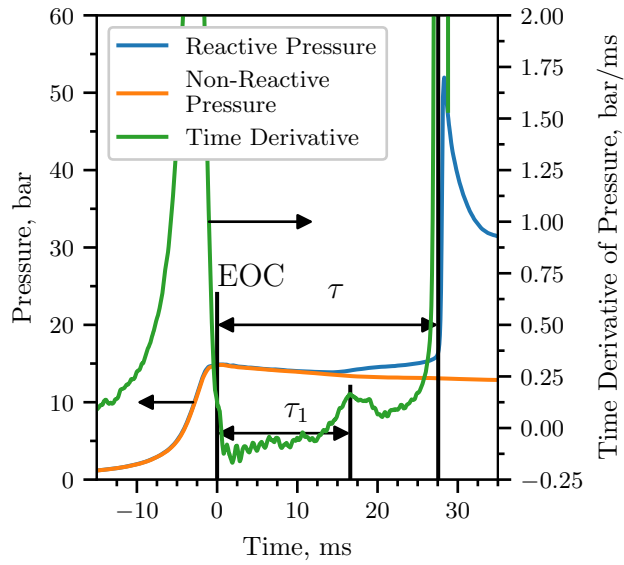
37 This work provides additional data for the autoignition of MV. Data is col-  
 38 lected in a RCM under engine relevant conditions spanning from 15 bar to 30 bar,  
 39 equivalence ratios ( $\phi$ ) from 0.25 to 2.0, and temperatures from 680 K to 1050 K.  
 40 The NTC region of MV is mapped out to provide additional information on the  
 41 fidelity of using MV as a biodiesel surrogate.

## 42 **2. Experimental Methods**

43 The RCM used in this study is a single piston arrangement and is pneu-  
 44 matically driven and hydraulically stopped. The device has been described in  
 45 detail previously [16] and will be described here briefly for reference. The end  
 46 of compression (EOC) temperature and pressure ( $T_C$  and  $P_C$  respectively), are  
 47 independently changed by varying the overall compression ratio, initial pressure  
 48 ( $P_0$ ), initial temperature ( $T_0$ ), and specific heat ratio of the experiments. The  
 49 piston in the reaction chamber is machined with a specially designed crevice to  
 50 suppress the roll-up vortex effect and promote homogeneous conditions in the  
 51 reactor during and after compression [17].

52 The primary diagnostic on the RCM is the in-cylinder pressure measured by  
 53 a Kistler 6125C dynamic transducer that is compensated for thermal shock. The  
 54 transducer is coupled to a Kistler 5010B charge amplifier. The voltage output

55 of the charge amplifier is recorded by a National Instruments 9125 analog input  
 56 device connected to a cDAQ 9178 chassis. The voltage is sampled at a rate of  
 57 either 50 kHz or 100 kHz by a LabView VI and processed by a Python package  
 58 called UConnRCMPy [18]. Version 3.0.5 of UConnRCMPy [19], 3.6 of Python,  
 59 2.3.0 of Cantera [20], 1.13.0 of NumPy [21], 0.19.0 of SciPy [22], and 2.0.1 of  
 60 Matplotlib [23] are used in the analysis in this paper.



61

Figure 1: Definition of the ignition delays used in this work. The experiment in this figure is conducted for a  $\phi = 2.0$  mixture with  $\text{Ar}/(\text{N}_2 + \text{Ar}) = 0.5$ ,  $P_0 = 0.7806$  bar,  $T_0 = 373$  K,  $P_C = 14.92$  bar,  $T_C = 720$  K,  $\tau = (27.56 \pm 0.89)$  ms, and  $\tau_1 = (16.60 \pm 0.46)$  ms.

63 The compression stroke of the RCM brings the fuel/oxidizer mixture to the  
 64 EOC conditions, and for suitable thermodynamic states, the mixture will ignite  
 65 after a delay period. The definitions of the ignition delays are shown in Fig. 1.  
 66 The time of the EOC is defined as the maximum of the pressure trace prior to  
 67 the start of ignition and the ignition delays are defined as the time from the EOC  
 68 until local maxima in the first time derivative of the pressure. Each experimental  
 69 condition is repeated at least five times to ensure repeatability of the data. As  
 70 there is some random scatter present in the data, the standard deviation ( $\sigma$ ) of

the ignition delays from the runs at a given condition is computed. Typically,  $\sigma$  is less than 10 % of the mean values of the overall ignition delay ( $\tau$ ) and the first stage ignition delay ( $\tau_1$ ).

In addition to the reactive experiments, non-reactive experiments are conducted by replacing  $O_2$  with  $N_2$  to determine the influence of machine-specific behavior on the experimental conditions and permit the calculation of the EOC temperature via the isentropic relations between pressure and temperature [24]. The EOC temperature is calculated by the procedure described in Section 3.

The mixtures considered in this study are shown in Table 1. Four equivalence ratios of MV in “air” are considered. While  $O_2$  is kept at 21 % by mole in the oxidizer, the ratio of Ar :  $N_2$  in the oxidizer is varied to adjust the temperatures reached at the EOC. Two  $P_C$  conditions are studied in this work, 15 bar and 30 bar, representing engine-relevant conditions. For the  $\phi = 2.0$  condition, only  $P_C = 15$  bar is considered because we could not achieve  $T_C$  values low enough that the ignition during the compression stroke can be prevented.

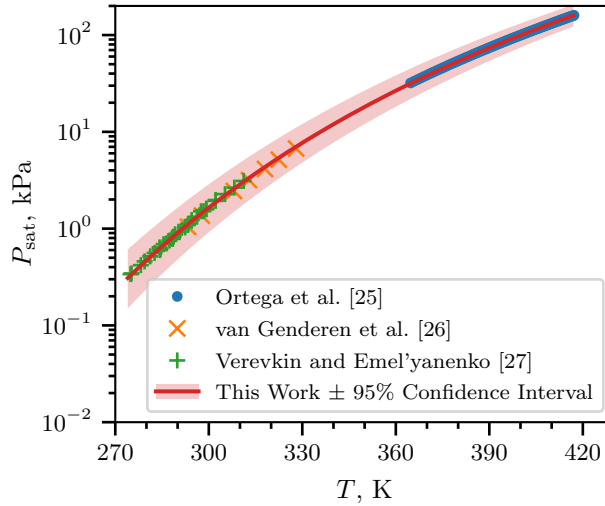
Table 1: Mixtures considered in this work

$\phi$	Mole Fraction (purity)				Ar/( $N_2 + Ar$ )
	MV (100 %)	$O_2$ (99.994 %)	Ar (99.999 %)	$N_2$ (99.999 %)	
0.25	0.0065	0.2087	0.7848	0.0000	1.0
0.5	0.0130	0.2074	0.7796	0.0000	1.0
1.0	0.0256	0.2047	0.7697	0.0000	1.0
1.0	0.0256	0.2047	0.3849	0.3848	0.5
2.0	0.0499	0.1996	0.0000	0.7505	0.0
2.0	0.0499	0.1996	0.3752	0.3753	0.5

Mixtures are prepared in stainless steel mixing tanks, 17 L and 15 L in size. The proportions of reactants in the mixture are determined by specifying the absolute mass of the fuel, the equivalence ratio, and the ratio of Ar :  $N_2$  in the oxidizer. Mixtures are made by first vacuuming the mixing tanks to an

94 ultimate pressure less than 5 Torr. Since MV is a liquid with a relatively small  
 95 vapor pressure at room temperature and pressure, it is measured gravimetrically  
 96 to within 0.01 g of the specified value. The fuel is injected into the mixing tank  
 97 through a septum. Proportions of O<sub>2</sub>, Ar, and N<sub>2</sub> are added manometrically at  
 98 room temperature and the total pressure is measured by an Omega Engineering  
 99 MMA100V10T2D0T4A6 type static pressure transducer. The same transducer  
 100 is used to measure the pressure of the reactants prior to an experiment.

101 The RCM is equipped with heaters to control the initial temperature of the  
 102 mixture. After filling in the components to the mixing tanks, the heaters are  
 103 switched on and the system is allowed 1.5 h to come to steady state. The mixing  
 104 tanks are also equipped with magnetic stir bars so the reactants are well mixed  
 105 for the duration of the experiments.



106

Figure 2: Saturated vapor pressure of MV as a function of temperature, plotted using the  
 107 Antoine equation, Eq. (1), with  $A = 6.4030$ ,  $B = 1528.69$ , and  $C = 52.881$ .

The initial temperature is chosen such that the saturated vapor pressure  
 ( $P_{\text{sat}}$ ) of the fuel at the initial temperature is at least twice the partial pressure

of the fuel in the mixing tank. The Antoine equation

$$\log_{10} P_{\text{sat}} = A - \frac{B}{T - C} \quad (1)$$

is used to model the saturated vapor pressure of MV as a function of temperature ( $T$ ), where  $A$ ,  $B$ , and  $C$  are substance-specific coefficients. Coefficients for Eq. (1) are given in the literature by Ortega et al. [25], Camacho et al. [28], and Stephenson et al. [29]. Unfortunately, the values of the coefficients are different among all three references. Therefore, coefficients for use in Eq. (1) are determined in this work by least squares fitting of the data of Ortega et al. [25], van Genderen et al. [26], and Verevkin and Emel'yanenko [27] using the `curve_fit()` function of SciPy [22] version 0.19.0. Figure 2 shows that the coefficients fitted with this procedure give good agreement with the experimental data; values for the coefficients computed in this work and in the literature works are given in Table 2. The data and code used to calculate the coefficients are provided in the Supplementary Material.

Table 2: Antoine Equation coefficients computed in this work and from the literature. The  $2\sigma$  confidence interval is estimated by taking the square root of the diagonals of the covariance matrix returned from `curve_fit()`

	$A$	$B$	$C$	$T_{\text{min}}$ , K	$T_{\text{max}}$ , K
This Work	6.4030	1528.69	52.881	274.9	417.18
$2\sigma$ Confidence Interval	0.0919	53.47	4.934	—	—
Ortega et al. [25]	6.23175	1429.00	62.30	364.75	417.18
Camacho et al. [28]	5.9644	1281.06	75.94	281	547
Stephenson et al. [29]	6.62646	1658.4	42.09	297	411

### 3. Computational Methods

#### 3.1. RCM Modeling

The Python 3.6 interface of Cantera [20] version 2.3.0 is used for all simulations in this work. Detailed descriptions of the use of Cantera for these

126 simulations can be found in the work of Weber and Sung [18] and Dames  
 127 et al. [30]; a brief overview is given here. As mentioned in Section 2, non-  
 128 reactive experiments are conducted to characterize the machine-specific effects  
 129 on the experimental conditions in the RCM. This pressure trace is combined  
 130 with the reactive pressure trace and used to compute a volume trace by as-  
 131 suming that the reactants undergo a reversible, adiabatic, constant composition  
 132 (i.e., isentropic) compression during the compression stroke and an isentropic  
 133 expansion after the EOC. The volume trace is applied to a simulation con-  
 134 ducted in an `IdealGasReactor` in Cantera [20] using the CVODES solver from  
 135 the SUNDIALS suite [31]. The ignition delays from the simulations are de-  
 136 fined in the same manner as in the experiments. The time derivative of the  
 137 pressure in the simulation is computed by second order Lagrange polynomials,  
 138 as discussed by Chapra and Canale [32]. The volume trace files, the corre-  
 139 sponding pressure traces, and `volume-trace.yaml` files suitable for use with  
 140 UConnRCMPy v3.0.5 [19] are available on the web at [https://combdialab.](https://combdialab.engr.uconn.edu/database/rcm-database)  
 141 [engr.uconn.edu/database/rcm-database](https://combdialab.engr.uconn.edu/database/rcm-database) and on figshare at [https://doi.](https://doi.org/10.6084/m9.figshare.5213341)  
 142 [org/10.6084/m9.figshare.5213341](https://doi.org/10.6084/m9.figshare.5213341). In addition, ChemKED-format [33] files  
 143 are available in the main ChemKED database repository at [https://github.](https://github.com/pr-ometh-us/ChemKED-database)  
 144 [com/pr-ometh-us/ChemKED-database](https://github.com/pr-ometh-us/ChemKED-database).

145 To the best of our knowledge, there are three mechanisms for MV com-  
 146 bustion available in the literature. The first two, by Korobeinichev et al. [12]  
 147 and Dmitriev et al. [13], were developed to simulate flames, and do not include  
 148 the low-temperature chemistry necessary to simulate the conditions in these ex-  
 149 periments. The third model was developed by Diévar et al. [15] and includes  
 150 low-temperature chemistry of MV, although it was only validated by comparison  
 151 with flame extinction limits. In converting this mechanism for use in Cantera,  
 152 we found that there were many species in the thermodynamic database with  
 153 multiple data entries. For most of these species the thermodynamic data is  
 154 identical. However, some species are not exact duplicates. For these species, it  
 155 is not clear from the thermodynamic database file which data set should be pre-  
 156 ferred. Since Cantera (and CHEMKIN) choose the first instance of a duplicate



species to be used, we retained the first entry for all duplicated species. The detailed model of Diévar et al. [15] includes 1105 species and 7141 reactions, and the Cantera formatted input file is available in the Supplementary Material.

### 3.2. Reaction Mechanism Generator

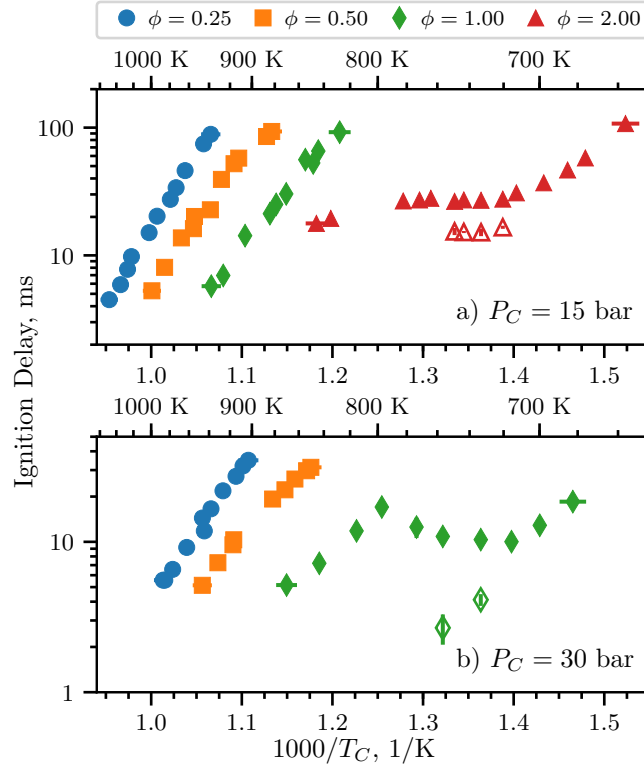
In addition to using a mechanism from the literature, we investigate the use of an automatic mechanism generator, the open-source Reaction Mechanism Generator (RMG) [34] version 2.1.0. The Python version of RMG is used, which requires Python 2.7, and version 2.1.0 of the RMG database is used. The final RMG model contains 427 species and 13640 reactions. Note that the number of species is much lower than the Diévar et al. [15] model because the RMG model focuses on only one fuel (MV), but the number of reactions is substantially higher. The input file used to generate the model is available in the Supplementary Material. In addition, the CHEMKIN and Cantera formatted input files for the RMG model are available in the Supplementary Material.

## 4. Experimental Results

### 4.1. Ignition Delays

Figure 3 shows the ignition delay results measured in this study. Filled markers denote the overall ignition delay and hollow markers indicate the first-stage ignition delay. Vertical error bars are drawn on the symbols to represent the  $2\sigma$  uncertainty in the ignition delay; for many of the experiments, the uncertainty is approximately the same size as the data point, so the error bar is hidden. Horizontal error bars are shown on the first and last points of each equivalence ratio indicating the estimated uncertainty in the EOC temperature of  $\pm 1\%$  [35]. Fig. 3a shows the results for a compressed pressure of 15 bar, while Fig. 3b shows the results for a compressed pressure of 30 bar. Note that  $\phi = 2.0$  results were not collected for 30 bar, so there are no red triangle data points in Fig. 3b. A summary of the ignition delay data is available as a comma-separated value file in the Supplementary Material.

185 It can be seen from Fig. 3 that the ignition delays for the  $\phi = 0.25$  and 0.5  
 186 mixtures do not show an NTC region of the ignition delay for both of the  
 187 pressures studied in this work. However, the  $\phi = 1.0$  mixture shows an NTC  
 188 region at  $P_C = 30$  bar between approximately 720 K and 800 K, with measured  
 189 first-stage ignition delays at 733 K and 757 K. In addition, the  $\phi = 2.0$  mixture  
 190 shows an NTC region of ignition delay at 15 bar from approximately 720 K to  
 191 780 K, with measured first-stage ignition delays between 720 K and 750 K.



192 Figure 3: Ignition delays of MV as a function of inverse temperature for varying equivalence  
 ratios. Filled points are the overall ignition delays and hollow points are the first stage ignition  
 193 delays. a) 15 bar, b) 30 bar.

194 Hadj-Ali et al. [9] also observed two-stage ignition of MV in stoichiometric  
 195 mixtures, stating that “[m]ethyl pentanoate... was more reactive [than methyl  
 196 butanoate] with a limit below which autoignition no longer occurs observed at  
 197  $T_c = 670$  K and  $P_c = 11.4$  bar. At this temperature, the autoignition occurred

in two stages with a clearly identified cool flame event.” However, we do not find two stage ignition for the similar pressure of  $P_C = 15$  bar in this study. We note that the stated temperature of the experiment from the work of Hadj-Ali et al. [9] (670 K) is much lower than the lowest temperature we considered in this work at 15 bar,  $\phi = 1.0$  (828 K). We did not conduct experiments at lower temperatures because the work of Mittal and Sung [17] showed that the temperature field in the RCM reaction chamber was uniform for approximately 100 ms after the EOC, and our measured ignition delay at 15 bar,  $\phi = 1.0$ , and 828 K is 92.14 ms.

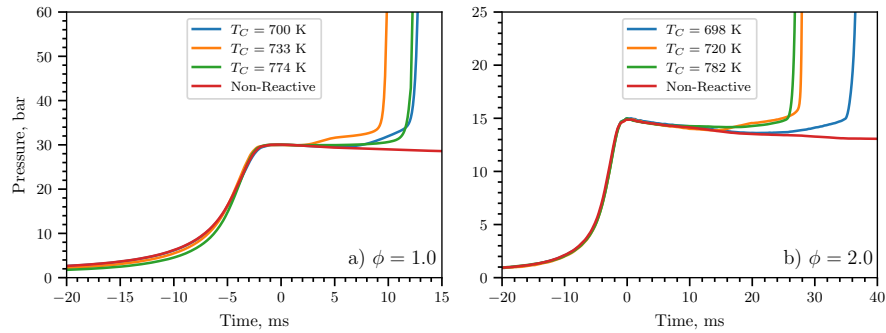
However, we note NTC behavior of the ignition delay and two-stage ignition at the higher pressure of 30 bar, and at higher temperatures than those reported for two-stage ignition in the study of Hadj-Ali et al. [9]. The trend of NTC behavior shifting to higher temperatures with increasing pressure can be seen in other classes of fuels. Kukkadapu et al. [36] found a similar trend in gasoline composed of iso-alkanes, n-alkanes, cyclo-alkanes, aromatics, and olefins. Kukkadapu et al. [36] attributed the shift of the NTC region to the reactions between the hydroperoxyalkyl radical (QOOH) and  $O_2$  becoming more dominant than the unimolecular decomposition of QOOH at higher pressures. Similar trends could occur for the hydroperoxyalkyl radicals of MV.

To further understand the effect of the methyl ester functional group on the NTC region of ignition delay, we compare with the alkane and alcohol with 5-carbon alkyl chains, n-pentane and n-pentanol. n-Pentane and MV have the same fuel mole percentage for stoichiometric mixtures in air (2.56 %), while n-pentanol has a fuel mole percentage of 2.72 % for stoichiometric conditions. Ribaucour et al. [37] and Bugler et al. [38] found the NTC region for n-pentane to be between 760 K and 910 K at pressures near 10 atm. As we will compare with our MV data at 30 bar, we note that increasing the pressure tends to shift the NTC to higher temperatures, as mentioned previously [36]. Heufer et al. [39] found NTC behavior for n-pentanol in the range of 770 K to 900 K at 30 bar. In this study, we find the NTC window for MV at 30 bar to be between 720 K and 800 K. Therefore, it appears that the methyl ester functional group causes the

229 NTC range to occur at lower temperature as compared to alkanes and alcohols  
 230 with similar alkyl chain lengths. This result was also noted by Hadj-Ali et al.  
 231 [9] for methyl hexanoate as the fuel.

#### 232 4.2. Pressure Traces

233 Figure 4a shows the pressure traces for selected experiments at  $\phi = 1.0$ ,  $P_C =$   
 234 30 bar. The three reactive pressure traces shown are at the low-temperature end  
 235 of the NTC (blue, 700 K), one case with two-stage ignition (orange, 733 K), and  
 236 one case near the high-temperature limit of the NTC region (green, 774 K). Also  
 237 shown is the non-reactive pressure trace for the 700 K case (red). By comparing  
 238 the 700 K pressure trace with the non-reactive pressure trace, it can be seen  
 239 that there is substantial heat release prior to main ignition as measured by the  
 240 deviation of the reactive pressure trace from the non-reactive trace. However,  
 241 there is only one peak in the time derivative of the pressure, so no first-stage  
 242 ignition delay is defined for this case. It can also be seen in Fig. 4a that the  
 243 774 K case shows some heat release prior to ignition, although again there is  
 244 only one peak in the time derivative of the pressure. Furthermore, the heat  
 245 release at 774 K appears to be more gradual than at 700 K.



246 Figure 4: Selected pressure traces around the NTC region of ignition delay. a)  $\phi = 1.0$ ,  $P_C =$   
 247 30 bar, b)  $\phi = 2.0$ ,  $P_C = 15$  bar

248  
 249 A similar trend can be observed in Fig. 4b for  $\phi = 2.0$  at  $P_C = 15$  bar,  
 250 where pressure traces at several points around the NTC region are plotted. As

in Fig. 4a, the three reactive pressure traces shown are at the low-temperature end of the NTC (blue, 698 K), one case with two-stage ignition (orange, 720 K), and one case near the high-temperature limit of the NTC region (green, 782 K). Also shown is the non-reactive pressure trace for the 698 K case (red). As for the  $\phi = 1.0$  case, the pressure traces show significant heat release prior to the overall ignition, as judged by deviation from the non-reactive case.

## 5. Computational Results

Figure 5 compares experimentally measured overall ignition delays with ignition delays computed with the detailed model of Diévar et al. [15] (solid lines). Figure 5a shows results at  $P_C = 15$  bar, while Fig. 5b shows results at  $P_C = 30$  bar. Only some equivalence ratios are shown for each pressure condition; data and simulated results are not shown for cases where the reactive simulated temperature at the EOC deviated substantially from the non-reactive temperature due to heat release during the compression stroke. Furthermore, it is important to note that the model of Diévar et al. [15] was not validated for MV ignition delays, only for extinction strain rates.

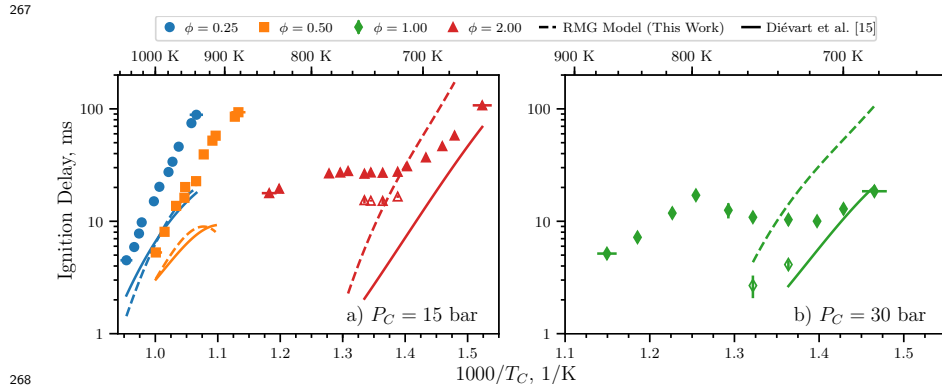


Figure 5: Comparison of experimental and simulated results. a) 15 bar, b) 30 bar

At 15 bar, the experimental ignition delays are under-predicted by the Diévar et al. [15] model for the three equivalence ratios shown. For the  $\phi = 0.25$  and 0.5

273 conditions, the model appears to be predicting an NTC region of the ignition  
 274 delays as the temperature decreases, although such a trend is not observed in the  
 275 data. However, at  $\phi = 2.0$ , the model does not predict the presence of an NTC  
 276 region, although one is present in the experiments. Nonetheless, the agreement  
 277 seems to be improving as the temperature is decreased. Comparing the Diévert  
 278 et al. [15] model to the stoichiometric data at 30 bar, we find a similar trend as  
 279 the  $\phi = 2.0$ ,  $P_C = 15$  bar data. The model does not predict the NTC region  
 280 found experimentally for the  $\phi = 1.0$  experiments, but the agreement improves  
 281 as the temperature decreases. Interestingly, two-stage ignition is predicted for  
 282 all of the  $\phi = 1.0$  and  $\phi = 2.0$  data shown in Fig. 5. However, the first-stage  
 283 ignition delays are 0.1 ms to 0.5 ms less than the overall ignition delays, and are  
 284 not shown on Fig. 5 because they are nearly indistinguishable from the overall  
 285 ignition delay. While the model of Diévert et al. [15] over-predicts the first-stage  
 286 ignition delay, it also over-predicts the first-stage pressure rise, thereby leading  
 287 to rapid overall ignition.

288 To elucidate the underlying reasons for the disagreement between the Diévert  
 289 et al. [15] model and the data, we constructed an additional model using RMG  
 290 (see Section 3.2). As can be seen in Fig. 5a, the agreement between the RMG  
 291 model (dashed lines) and the experimental data is similar to the Diévert et al.  
 292 [15] model for the 15 bar,  $\phi = 0.25$  and 0.5 data. Moreover, the RMG model  
 293 predicts a similar NTC region as temperature is decreasing. For the 15 bar,  
 294  $\phi = 2.0$  data, the RMG model tends to over-predict the low-temperature ignition  
 295 delays, and does not predict the NTC region found experimentally. As before,  
 296 the trend at 30 bar,  $\phi = 1.0$  is similar to the 15 bar,  $\phi = 2.0$  data; the RMG  
 297 model over-predicts the low-temperature ignition delays and does not predict  
 298 the experimental NTC region. Finally, as in the Diévert et al. [15] model, two-  
 299 stage ignition is predicted for all of the  $\phi = 1.0$  and  $\phi = 2.0$  data shown in  
 300 Fig. 5. However, the first-stage ignition delays are 0.1 ms to 0.5 ms less than  
 301 the overall ignition delays, and are not shown on Fig. 5 because they are nearly  
 302 indistinguishable from the overall ignition delay. Again, the over-prediction of  
 303 the first-stage ignition delay and pressure rise requires further investigation and

304 understanding of the complex low-temperature chemistry.

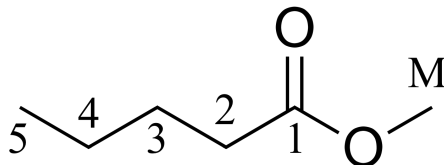
305 It is clear that neither model is able to predict the ignition delays of MV  
306 particularly well. In addition to the poor agreement shown in Fig. 5, the simu-  
307 lations for  $P_C = 15$  bar,  $\phi = 1.0$  and  $P_C = 30$  bar,  $\phi = 0.25, 0.5$  and  $2.0$  showed  
308 substantial heat release during the compression stroke (i.e., the simulations are  
309 much too reactive), and so these conditions aren’t compared in Fig. 5. We note  
310 again that the model by Diévar et al. [15] was validated for MV combustion  
311 only by comparison to flame extinction limits, so the disagreement is not wholly  
312 surprising.

313 In general, there could be three likely sources of error in the models: missing  
314 reaction pathways, incorrect values of the reaction rates, and incorrect values  
315 for thermodynamic properties of the species. We have noted in Section 3.2 that  
316 the RMG model has many more reactions than the Diévar et al. [15] model  
317 and the algorithm used in RMG considers a substantial number of the possible  
318 pathways. This reduces the possibility of missing reaction pathways affecting  
319 the model. Further detailed studies are required to ensure that the RMG model  
320 includes all of the relevant reaction pathways, which are outside the scope of  
321 this work.

322 The second source of error may be incorrect reaction rate parameters, either  
323 because the rates are specified incorrectly in the model or because the rates are  
324 not well estimated by the typical analogy based-rules. It should be noted that  
325 errors of this type may affect the model generated by RMG—if the rates are not  
326 estimated correctly, reactions that are important in reality may not be included  
327 in the model. Determining the accuracy of the reaction rates used in the RMG  
328 and Diévar et al. [15] models requires further detailed studies of the models,  
329 which are also outside the scope of this work. Another, related, source of error  
330 could be incorrect estimation of the pressure dependence of the reaction rates,  
331 which may be particularly important for the isomerization reactions prevalent  
332 in low-temperature chemistry.

333 The third source of error may lie in the estimation of the thermodynamic  
334 properties of the species, particularly the fuel radicals. In the work of Diévar

et al. [15], the program THERM [40] is used to estimate thermodynamic values using the group additivity method. In the RMG model constructed in this work, RMG itself estimates the thermodynamic properties of the molecules also using the group additivity method. Nonetheless, the two models have differing predictions of the thermodynamic properties of the species in the model, particularly the fuel and its radicals. The values of the heats of formation of the fuel and its H-atom abstraction radicals are shown in Table 3; the radicals are labeled according to the convention shown in Fig. 6.



343

Figure 6: Structure of MV with carbon atoms labeled according to the convention used in Table 3 and Table 4

Table 3: Heats of formation of MV and its radicals, labeled according to the convention used in Fig. 6

345

Radical Site	Diévert et al. [15]		RMG Model (this work)	
	[kJ/mol]	[kcal/mol]	[kJ/mol]	[kcal/mol]
MV	-470.98	-112.57	-472.53	-112.94
2	-297.16	-71.02	-273.63	-65.40
3	-277.03	-66.21	-273.63	-65.40
4	-277.03	-66.21	-278.61	-66.59
5	-265.94	-63.56	-267.53	-63.94
M	-270.51	-64.65	-270.12	-64.56

346

Table 3 shows that the heats of formation of the fuel and radicals 3, 4, 5, and M are quite similar between the two mechanisms. However, the heat of formation of the second radical, the one closest to the methyl ester group, has a significantly lower heat of formation in the model by Diévert et al. [15]

350



than in the RMG model. Note that it is expected that the second radical will be somewhat more stable than the other radicals, due to the influence of the methyl ester group on the adjacent carbon atom.

This difference in heats of formation affects the pathways that consume the fuel. By conducting a reaction pathway analysis to determine which radicals are formed from the breakdown of the fuel, we can analyze the proportion of each radical formed as the fuel breaks down during the autoignition process. The following analysis is conducted for a constant volume, adiabatic simulation with initial temperature and pressure of 700 K, 30 bar, and for the stoichiometric equivalence ratio. The rates of production of the species have been integrated until the time of 20 % fuel consumption. The results of this analysis are shown in Table 4 for the two models. The percentages shown in the Table 4 are the percent of the fuel consumed to form a particular fuel radical by all the reactions that can form that radical, and the radicals are labeled according to the convention in Fig. 6.

Table 4: Percent of MV consumed to form fuel radical species with a hydrogen atom missing at the location indicated in the first column and Fig. 6

Radical Site	Diévert et al. [15] [%]	RMG Model [%]	RMG switched [%]
2	29.2	12.5	11.0
3	17.5	12.2	11.1
4	17.5	50.6	56.6
5	9.5	3.9	4.3
M	26.3	20.8	16.9

At the relatively low temperature and high pressure condition of this analysis, all of the fuel is consumed by H-atom abstractions to form the fuel radicals shown. It can be seen that the two models have quite different distributions of products from the first H-abstraction reactions. The model of [15] predicts that H-abstraction from the second carbon is the most prevalent, while the RMG model predicts that the radical on the fourth carbon in the chain will be primarily formed. This is in line with the heats of formation in Table 3, where

the most stable radical (i.e., the radical with the smallest heat of formation) is most likely to be formed in each model.

To further compare the models with each other, the NASA polynomials representing the thermodynamic properties of MV and the 5 fuel radicals from the model of Diévar et al. [15] and are used to replace the equivalent molecules in the RMG model. The results of a path analysis at the same condition as the other analysis is shown in Table 4 in the “RMG switched” column. This analysis shows that the radical on the fourth carbon atom is still the most prevalent, despite changing the heats of formation of the fuel and its radicals.

Taken together, these results show that the poor performance in a given model cannot be attributed to a single source. There is a strong interaction between the thermodynamics of the species and the kinetics of the reactions, requiring further detailed study of the methyl ester system to accurately predict the low temperature ignition delays of methyl valerate.

## 6. Conclusions

In this study, we have measured ignition delays for methyl valerate over a wide range of engine-relevant pressures, temperatures, and equivalence ratios. An NTC region of the ignition delay and two-stage ignition are recorded for pressures of 15 bar at  $\phi = 2.0$  and 30 bar at  $\phi = 1.0$ . A detailed chemical kinetic model available in the literature is unable to reproduce the experimental results, so a new model is constructed using the Reaction Mechanism Generator software. Although the new model contains many more reactions than the literature model, it is still unable to predict the experimental ignition delays satisfactorily. Both models predict an NTC region of the ignition delay under conditions where none is found in the experiments, and fail to predict the NTC region of ignition delay that is present in the experiments. Possible reasons for the discrepancy include missing reaction pathways, incorrect rate estimates, and incorrect thermodynamic property estimates. Comparative analysis of the two models failed to identify a single source of the error, and further detailed studies

are required to improve predictions of the ignition delay at these engine-relevant conditions.

## 7. Acknowledgments

The authors acknowledge support from the Combustion Energy Frontier Research Center, an Energy Frontier Research Center funded by the U.S. Department of Energy, Office of Science, Office of Basic Energy Sciences, under award number DE-SC0001198.

## References

- [1] S. K. Hoekman, C. Robbins. Review of the effects of biodiesel on NO<sub>x</sub> emissions. *Fuel Processing Technology* 96 (2012) 237–249. doi:10.1016/j.fuproc.2011.12.036.
- [2] J. Y. Lai, K. C. Lin, A. Violi. Biodiesel combustion: Advances in chemical kinetic modeling. *Progress in Energy and Combustion Science* 37 (2011) 1–14. doi:10.1016/j.pecs.2010.03.001.
- [3] L. Coniglio, H. Bennadji, P. Glaude, O. Herbinet, F. Billaud. Combustion chemical kinetics of biodiesel and related compounds (methyl and ethyl esters): Experiments and modeling – Advances and future refinements. *Progress in Energy and Combustion Science* 39 (2013) 340–382. doi:10.1016/j.pecs.2013.03.002.
- [4] W. K. Metcalfe, S. Dooley, H. J. Curran, J. M. Simmie, A. M. El-Nahas, M. V. Navarro. Experimental and modeling study of C<sub>5</sub>H<sub>10</sub>O<sub>2</sub> ethyl and methyl esters. *The Journal of Physical Chemistry A* 111 (2007) 4001–4014. doi:10.1021/jp067582c.
- [5] S. M. Walton, M. S. Wooldridge, C. K. Westbrook. An experimental investigation of structural effects on the auto-ignition properties of two C<sub>5</sub> esters. *Proceedings of the Combustion Institute* 32 (2009) 255–262. doi:10.1016/j.proci.2008.06.208.

- [6] S. Dooley, H. J. Curran, J. M. Simmie. Autoignition measurements and a validated kinetic model for the biodiesel surrogate, methyl butanoate. *Combustion and Flame* 153 (2008) 2–32. doi:10.1016/j.combustflame.2008.01.005.
- [7] B. Akih-Kumgeh, J. M. Bergthorson. Comparative Study of Methyl Butanoate and n -Heptane High Temperature Autoignition. *Energy & Fuels* 24 (2010) 2439–2448. doi:10.1021/ef901489k.
- [8] B. Akih-Kumgeh, J. M. Bergthorson. Structure-reactivity trends of C1–C4 alkanolic acid methyl esters. *Combustion and Flame* 158 (2011) 1037–1048. doi:10.1016/j.combustflame.2010.10.021.
- [9] K. Hadj-Ali, M. Crochet, G. Vanhove, M. Ribaucour, R. Minetti. A study of the low temperature autoignition of methyl esters. *Proceedings of the Combustion Institute* 32 (2009) 239–246. doi:10.1016/j.proci.2008.09.002.
- [10] K. Kumar, C.-J. Sung. Autoignition of methyl butanoate under engine relevant conditions. *Combustion and Flame* 171 (2016) 1–14. doi:10.1016/j.combustflame.2016.04.011.
- [11] E. Fisher, W. J. Pitz, H. J. Curran, C. K. Westbrook. Detailed chemical kinetic mechanisms for combustion of oxygenated fuels. *Proceedings of the Combustion Institute* 28 (2000) 1579–1586. doi:10.1016/S0082-0784(00)80555-X.
- [12] O. Korobeinichev, I. Gerasimov, D. Knyazkov, A. Shmakov, T. Bolshova, N. Hansen, C. K. Westbrook, G. Dayma, B. Yang. An Experimental and Kinetic Modeling Study of Premixed Laminar Flames of Methyl Pentanoate and Methyl Hexanoate. *Zeitschrift für Physikalische Chemie* 229 (2015). doi:10.1515/zpch-2014-0596.
- [13] A. M. Dmitriev, D. A. Knyazkov, T. A. Bolshova, A. G. Shmakov, O. P. Korobeinichev. The effect of methyl pentanoate addition on

- the structure of premixed fuel-rich n-heptane/toluene flame at atmospheric pressure. *Combustion and Flame* 162 (2015) 1964–1975. doi:10.1016/j.combustflame.2014.12.015.
- [14] C. Hayes, D. R. Burgess. Exploring the oxidative decompositions of methyl esters: Methyl butanoate and methyl pentanoate as model compounds for biodiesel. *Proceedings of the Combustion Institute* 32 (2009) 263–270. doi:10.1016/j.proci.2008.05.075.
- [15] P. Diévert, S. H. Won, J. Gong, S. Dooley, Y. Ju. A comparative study of the chemical kinetic characteristics of small methyl esters in diffusion flame extinction. *Proceedings of the Combustion Institute* 34 (2013) 821–829. doi:10.1016/j.proci.2012.06.180.
- [16] G. Mittal, C.-J. Sung. A Rapid Compression Machine for Chemical Kinetics Studies at Elevated Pressures and Temperatures. *Combustion Science and Technology* 179 (2007) 497–530. doi:10.1080/00102200600671898.
- [17] G. Mittal, C.-J. Sung. Aerodynamics inside a rapid compression machine. *Combustion and Flame* 145 (2006) 160–180. doi:10.1016/j.combustflame.2005.10.019.
- [18] B. W. Weber, C.-J. Sung. UConnRCMPy: Python-based Data Analysis for Rapid Compression Machines. in: S. Benthall, S. Rostrup (Eds.), *Proceedings of the 15th Python in Science Conference*, pp. 36–44. [http://conference.scipy.org/proceedings/scipy2016/bryan\\_weber.html](http://conference.scipy.org/proceedings/scipy2016/bryan_weber.html).
- [19] B. W. Weber, R. Fang, C.-J. Sung. UConnRCMPy, 2017. v3.0.5. doi:10.5281/zenodo.815569.
- [20] D. G. Goodwin, H. K. Moffat, R. L. Speth. Cantera: An Object-oriented Software Toolkit for Chemical Kinetics, Thermodynamics, and Transport Processes, 2017. v2.3.0. doi:10.5281/zenodo.170284.

- [21] S. van der Walt, S. C. Colbert, G. Varoquaux. The NumPy Array: A Structure for Efficient Numerical Computation. *Computing in Science & Engineering* 13 (2011) 22–30. doi:10.1109/MCSE.2011.37.
- [22] E. Jones, T. Oliphant, P. Peterson, et al. SciPy: Open source scientific tools for Python, 2001–. <https://scipy.org>.
- [23] J. D. Hunter. Matplotlib: A 2D Graphics Environment. *Computing in Science & Engineering* 9 (2007) 90–95. doi:10.1109/MCSE.2007.55.
- [24] D. Lee, S. Hochgreb. Rapid Compression Machines: Heat Transfer and Suppression of Corner Vortex. *Combustion and Flame* 114 (1998) 531–545. doi:10.1016/S0010-2180(97)00327-1.
- [25] J. Ortega, F. Espiau, J. Tojo, J. Canosa, A. Rodríguez. Isobaric Vapor-Liquid Equilibria and Excess Properties for the Binary Systems of Methyl Esters + Heptane. *Journal of Chemical & Engineering Data* 48 (2003) 1183–1190. doi:10.1021/jc030117d.
- [26] A. C. van Genderen, J. van Miltenburg, J. G. Blok, M. J. van Bommel, P. J. van Ekeren, G. J. van den Berg, H. A. Oonk. Liquid–vapour equilibria of the methyl esters of alkanolic acids: Vapour pressures as a function of temperature and standard thermodynamic function changes. *Fluid Phase Equilibria* 202 (2002) 109–120. doi:10.1016/S0378-3812(02)00097-3.
- [27] S. P. Verevkin, V. N. Emel’yanenko. Transpiration method: Vapor pressures and enthalpies of vaporization of some low-boiling esters. *Fluid Phase Equilibria* 266 (2008) 64–75. doi:10.1016/j.fluid.2008.02.001.
- [28] A. G. Camacho, J. M. Moll, S. Canzonieri, M. A. Postigo. Vapor-Liquid Equilibrium Data for the Binary Methyl Esters (Butyrate, Pentanoate, and Hexanoate) (1) + Propanenitrile (2) Systems at 93.32 kPa. *Journal of Chemical & Engineering Data* 52 (2007) 871–875. doi:10.1021/jc060469v.
- [29] R. M. Stephenson, S. Malanowski, D. Ambrose, *Handbook of the Thermodynamics of Organic Compounds*, Elsevier, New York, 1987.

- [30] E. E. Dames, A. S. Rosen, B. W. Weber, C. W. Gao, C.-J. Sung, W. H. Green. A detailed combined experimental and theoretical study on dimethyl ether/propane blended oxidation. *Combustion and Flame* 168 (2016) 310–330. doi:10.1016/j.combustflame.2016.02.021.
- [31] A. C. Hindmarsh, P. N. Brown, K. E. Grant, S. L. Lee, R. Serban, D. E. Shumaker, C. S. Woodward. SUNDIALS: Suite of nonlinear and differential/algebraic equation solvers. *ACM Transactions on Mathematical Software* 31 (2005) 363–396. doi:10.1145/1089014.1089020.
- [32] S. C. Chapra, R. P. Canale, *Numerical Methods for Engineers*, McGraw-Hill Higher Education, Boston, 6th ed edition, 2010.
- [33] B. W. Weber, K. E. Niemeyer. ChemKED: A human- and machine-readable data standard for chemical kinetics experiments. Submitted to: *International Journal of Chemical Kinetics* (2017). [arXiv:1706.01987](#).
- [34] J. W. Allen, C. F. Goldsmith, W. H. Green. Automatic estimation of pressure-dependent rate coefficients. *Physical Chemistry Chemical Physics* 14 (2012) 1131–1155. doi:10.1039/c1cp22765c.
- [35] B. W. Weber, C.-J. Sung, M. W. Renfro. On the uncertainty of temperature estimation in a rapid compression machine. *Combustion and Flame* 162 (2015) 2518–2528. doi:10.1016/j.combustflame.2015.03.001.
- [36] G. Kukkadapu, K. Kumar, C.-J. Sung, M. Mehl, W. J. Pitz. Experimental and surrogate modeling study of gasoline ignition in a rapid compression machine. *Combustion and Flame* 159 (2012) 3066–3078. doi:10.1016/j.combustflame.2012.05.008.
- [37] M. Ribaucour, R. Minetti, L. R. Sochet. Autoignition of n-pentane and 1-pentene: Experimental data and kinetic modeling. *Symposium (International) on Combustion* 27 (1998) 345–351. doi:10.1016/S0082-0784(98)80422-0.

- 540 [38] J. Bugler, K. P. Somers, E. J. Silke, H. J. Curran. Revisiting the Ki-  
541 netics and Thermodynamics of the Low-Temperature Oxidation Pathways  
542 of Alkanes: A Case Study of the Three Pentane Isomers. *The Journal of*  
543 *Physical Chemistry A* 119 (2015) 7510–7527. doi:10.1021/acs.jpca.5b00837.
- 544 [39] K. A. Heufer, J. Bugler, H. J. Curran. A comparison of longer alkane  
545 and alcohol ignition including new experimental results for n-pentanol and  
546 n-hexanol. *Proceedings of the Combustion Institute* 34 (2013) 511–518.  
547 doi:10.1016/j.proci.2012.05.103.
- 548 [40] E. R. Ritter, J. W. Bozzelli. THERM: Thermodynamic property estimation  
549 for gas phase radicals and molecules. *International Journal of Chemical*  
550 *Kinetics* 23 (1991) 767–778. doi:10.1002/kin.550230903.